A Statistical Mechanics Study of Ring Size, Ring Shape, and the Relation to Pores Found in Zeolites

Robin A. Curtis and Michael W. Deem*

Department of Bioengineering and Department of Physics & Astronomy, Rice University, 6100 Main Street-MS 142, Houston, Texas 77005-1892

Received: November 12, 2002; In Final Form: May 23, 2003

In this work, we survey the size and flatness of rings that occur in known zeolites and also in a set of hypothetical structures. The results suggest that 16-membered rings, while rarely observed in zeolites, are not unique and should be thermodynamically accessible. Conversely, the results also show that rings of a given flatness, or planarity, become exponentially less likely as ring size increases. We compare the geometry of rings in known zeolites with the geometry of unconstrained rings as determined from Monte Carlo simulation. The rings that occur in zeolites are flatter than unconstrained rings due to the constraints imposed by the crystal. The thermodynamic factors that determine the flatness of rings in crystals is investigated by using a reverse umbrella sampling technique. Interestingly, the energy required to bring rings from an unconstrained state to the crystalline flat state is roughly 5 kJ/mol Si, which is similar to the range of stabilities observed for zeolites and also to the range of interaction energies between zeolites and structure-directing agents.

1. Introduction

Zeolites are microporous crystalline materials composed mainly of Al and Si atoms (termed T-atoms), each of which is tetrahedrally connected to O atoms. Each O atom is either shared between adjacent tetrahedra or is a terminal group. Because zeolites are crystalline, they contain a sharp distribution of pore sizes. Consequently, zeolites have many applications where size and shape selectivity is required, such as in catalysis, ion-exchange, and adsorption. It is of interest to form zeolites with larger pores to perform shape-selective processes on molecules with sizes greater than 8 Å.[1,2] However, synthesis of zeolites containing larger pores is more complicated because the organocations most commonly used as structure directing agents are small. Synthesis of wider pores requires larger organocations; unfortunately controlling the crystallization product under these conditions is more difficult.[3]

Zeolite pores are classified by the number of T-atoms contained in the rings that surround the pores. Zeolites containing pores circumscribed by rings containing 8, 10, and 12 T-atoms are considered as small, medium, and large-pore zeolites. For example, the 12-membered ring in zeolite NaX surrounds a pore of 8 Å. The search for larger-pored zeolites was motivated by the discovery of VFI (VPI-5). VFI is an aluminophosphate containing 12 Å diameter pores circumscribed by 18-membered rings. Unfortunately, aluminophosphates are not as useful as aluminosilicates due to limited thermal stability with respect to water vapor, although there are at least a couple of commercialized aluminophosphates—CHA (SAPO-34) and AEL (SAPO-11). In the past few years, two zeolites containing 14-membered rings were synthesized, DON (UTD-1)[4] and CFI (CIT-5)[5] with pore apertures of 8.1 and 7.4 Å, respectively. In addition, two zeolites, SSZ-44 and SSZ-35, have been synthesized with pores surrounded by alternating rings containing 10 and 18 members.[6] However, both of these zeolites exhibit shape selective activity characteristic of apertures surrounded by the 10-membered rings. There has also been a focus on producing mesoporous aluminosilicates using surfactants as the structure-directing agents. To date, these efforts have not been proven to produce materials with a high degree of crystallinity.[2]

Understanding the thermodynamic and kinetic factors that govern the formation of different porous networks may aid in choosing conditions for the synthesis of specific zeolites. The free energies of formation for a set of all-silica zeolites fall in a narrow range with respect to thermal energy, indicating theoretically that it should be possible to synthesize many large-pore zeolite structures that do not violate the constraints of aluminosilicate chemistry.[7,8] The existing diversity of zeolite structures is due to the broad range of available synthesis conditions, including temperature, pH, salt concentration and type, and framework-atom composition. Understanding the kinetics may aid in choosing conditions favorable for the synthesis of desirable zeolitic structures. Unfortunately, the size of the critical nuclei is in a range that is difficult to measure experimentally—too large for NMR and too small for scattering. The rarity of the nucleation event poses another experimental difficulty. These challenges have motivated the use of simulation methods to study the crystallization process.[9] Novel algorithms are required to simulate zeolite nucleation because crystallization is a rare process and also because special reactive moves are required to break and make bonds.

In the first part of this work, we determine the size and flatness distribution of rings from a set of zeolites that contain either pure Si or a mixture of Si and Al as the T-atoms. In addition, we include in our study the aluminophosphate molecular sieves AET and VFI. As discussed later, although only a few rings containing greater than 12 T-atoms have been reported, there is an abundance of these rings that are not reported because the rings do not circumscribe pores. In addition, we determine the flatness of rings because it is found that for rings surrounding pores, flatter rings lead to larger openings. We classify rings that circumscribe pores as tabulated and all

* Corresponding author. E-mail: mwdeem@rice.edu. Fax: 713-348-5811.

10.1021/jp027447+ CCC: $25.00
Published on Web 07/12/2003

others as nontabulated. The measure of ring flatness discriminates between tabulated and nontabulated rings, since tabulated rings are generally more planar than nontabulated rings.

We also generate over 1800 hypothetical zeolite structures using the unit cell size parameters and the space group symmetries of known zeolites.[10,11] Given these constraints, we sample the possible positions of the unique T-atoms in the primary unit cell as well as the possible densities. The size and flatness distribution of rings in the hypothetical zeolites are compared to those in the known zeolites. The existence of hypothetical structures suggests that it may be possible to synthesize new zeolites with unique pore-size properties.

In the second part of the work, we perform Monte Carlo simulations of unconstrained rings to determine the preferred orientations of rings in the absence of the surrounding crystalline environment. Rings sample a different volume of phase space when the constraints imposed by allowable crystal structures are relaxed. From the simulations, we determine the contribution to the geometry of the ring arising from intramolecular interactions within the ring. The difference between the distribution of orientations in the crystal and that for the unconstrained ring is related to the interaction of the atoms in the ring with the atoms in the surroundings. These interactions with the surroundings produce an averaged crystalline potential that we measure as a function of the flatness of the ring.

The remainder of the article is organized as follows. In section 2 we present the method for determining a histogram of ring size distributions. In addition, we define the flatness order parameter in this section. The details of the Monte Carlo simulation of rings are given in section 3. In section 4, the results are discussed, followed by the conclusions in section 5.

2. Characterization of Rings in Zeolites

2.1. Hypothetical Zeolite Structure Generation. Zeolite structures that contain only four-coordinated T-atoms are uniquely determined by specifying the unit cell parameters, space group symmetry, and the positions of the unique T-atoms in the primary unit cell. The structures of all known zeolites have been solved by our group using the program ZEFSA[11] or ZEFSAII.[10] The required inputs for ZEFSA are the parameters describing the shape and size of the unit cell, the space group symmetry, number of unique T-atoms, and the X-ray powder diffraction data if available. In this method, a zeolite figure of merit is minimized using a biased Monte Carlo algorithm. The zeolite figure of merit includes geometric contributions from a two-body and a three-body potential of mean force among T-atoms and additional weighting factors that minimize the difference in calculated and expected density and four-connectedness of T-atoms. A scattering contribution that minimizes the difference between calculated and observed powder X-ray diffraction data can also be included. The Hamiltonian, or "cost function," in ZEFSA is roughly correlated with the thermodynamic energy, and the method has been very successful in generating correct zeolite structures. In this work, we use ZEFSAII to generate additional hypothetical zeolite structures that have the same space-group symmetry and unit cell parameters, but different unique T-atom positions and possibly different densities, as the known zeolites. We use only the geometric terms, no scattering data. We expect that the hypothetical structures have similar stabilities to known zeolites because the figure of merit corresponding to hypothetical structures is similar to that of the known structures.

2.2. Calculating Ring Histograms. A ring is defined as a closed loop of interconnecting links where the endpoints of each link correspond to the positions of two T-atoms that are bound to a common oxygen atom. A fundamental ring is defined as a ring that cannot be divided into a set of smaller rings.[12] This criterion is implemented by requiring that the minimum path distance between any two atoms in a fundamental ring is given by the topological distance separating the atoms on the ring. We determine the number of rings for a zeolite, considering the primary unit cell and the unit cells located on all corners and sides of the primary unit cell. The ring-size distribution histograms are generated by including only the fractions of the rings that are in the primary unit cell. The rings are classified as either tabulated or nontabulated by inspection of the position of the ring in the crystal structure. Tabulated rings are those rings that circumscribe a pore. A ring is automatically classified as nontabulated if a ring of that size is not reported in the IZA database.[13] For rings of a given size, we determine histograms of the flatness parameter defined in the next section. The flatness parameter defined below is used to discriminate between tabulated rings and nontabulated rings.

2.3. Flatness Parameter. The flatness parameter is determined from the T-atom distribution tensor, M, where the tensor elements are defined by

$$M^{\alpha\beta} = \sum_{i=1}^{N} \delta r_i^{\alpha} \delta r_i^{\beta} \tag{1}$$

Here, $\delta r_i^{\alpha} = r_i^{\alpha} - N^{-1}\sum_{j=1}^{N} r_j^{\alpha}$, where r_i^{α} is the α-component of the position vector for atom i in the laboratory frame. The sum includes only the N T-atom members of the ring and is independent of the identity of the T-atoms. Diagonalization of M corresponds to changing the coordinate axis from the laboratory frame to the body frame. The eigenvalues of the diagonalized matrix are given by

$$\lambda_{\alpha} = \sum_{i=1}^{N} \delta \bar{r}_i^{\alpha 2} \tag{2}$$

where the overbar denotes that the α-component of the position vector of atom i is with respect to the body axis. Subscript α also labels the eigenvalue, which we label in order of decreasing magnitude. Thus, λ_{α} is the mean square distance of the atoms in the ring in direction α of the body axis. We choose the flatness parameter, z, as

$$z = 1 - \left(\frac{\lambda_3}{\lambda_1}\right)^{1/2} \tag{3}$$

where λ_3 and λ_1 are the smallest and the largest eigenvalues of M, respectively. The term $(\lambda_3/\lambda_1)^{1/2}$ is approximately the ratio of the smallest width of the ring to the largest distance across the ring. For a planar ring, $\lambda_3 = 0$ and z is unity because the mean square distance of the ring atoms in the direction normal to the plane is zero. In the limit of a spherical, crumpled ring, the distribution of ring atoms about each axis is the same, $\lambda_1 = \lambda_2 = \lambda_3$, and z is equal to zero. A fairly flat ring, such as the 18-membered ring in VFI (VPI−5), has a flatness of $z = 0.9$.

3. Monte Carlo Simulations

3.1. Force Fields. We also study an unconstrained silicate ring in free solution. Silicate clusters have been studied previously using ab initio methods and classical force fields.[14−17] These methods have been used to study the reactivities and conformations of small clusters which have been observed experimentally in pre-synthesis gels containing silicate species.

Moreover, ring clusters are some of the standard secondary building units of zeolites.[17−19] Because ab initio methods are time-consuming, usually only a few different conformations of each small cluster are studied. These results are extrapolated to larger systems by using classical force fields that are fit to the results of the ab initio calculations on small clusters.[20] These force fields usually contain two-body and sometimes three-body interactions. In this work, we sample a continuous distribution of conformations of the ring clusters, which requires us to use a classical force field. Here, we choose to use a two- and three-body potential which has been successfully used to model the dynamical and structural properties of amorphous silica.[21] In addition, surface properties of quartz derived from ab initio calculations have been reproduced using this classical potential.[22] Because the Vashashita potential was originally used to simulate bulk systems of amorphous silica, there is only one type of O atom, where the partial charge on the 2-connected O atoms is one-half that on the Si atoms. However, the unconstrained clusters studied here do not have a 2:1 ratio of O to Si atoms because the clusters contain a large percentage of 1-connected terminal O atoms. This effect is accounted for by adjusting the charge on the 1-connected O atoms so that the cluster is electroneutral, to the value of $-0.40\ |e^-|$. The zero net charge environment should best mimic the conditions in all-silica zeolites, where there is no net charge in the absence of defect sites.

3.2. Hybrid Monte Carlo Method. We use the hybrid Monte Carlo method to equilibrate the silicate rings. This method has been used by Brotz and dePablo[23] and by Wu and Deem[9] to equilibrate dense systems containing Si and O atoms. The Hybrid Monte Carlo method combines the advantages of molecular dynamics and Monte Carlo methods. In the HBMC method, global moves are proposed on the basis of trajectories determined from integrating Newton's laws of motion. Unlike molecular dynamics, the HBMC method does not suffer from finite-size step errors. Before each Monte Carlo move, an initial velocity distribution is generated according to a Maxwellian distribution. The new trial coordinates are generated by solving Hamilton's equations using a time-reversible discretization scheme. After N integration steps, the move from state o to state n is accepted with a probability given by

$$P_{o\to n} = \min\{1,\exp[-\beta(H_n - H_o)]\} \tag{4}$$

where $\beta = 1/(k_B T)$ is the reciprocal temperature and H is the Hamiltonian given by the sum of the kinetic energy and the potential energy. The average discretization error, $H_n - H_o$, increases with $N\delta t$ where δt is the size of the time step. Consequently, if $N\delta t$ is too large, the acceptance probability will be low. In this work, each Monte Carlo move involves 10 particle position updates with a time step of approximately 5 fs to give an acceptance probability of roughly eighty percent. The velocity Verlet algorithm is used as the discretization scheme.

3.3. Flatness Parameter. Flatness parameter histograms are generated from the simulations where the histograms simply measure how likely it is for a ring to be of a certain flatness. The flatness parameter distribution is given by

$$p(z') = \frac{\int d\mathbf{r}_{Si}^{n_{Si}}\, d\mathbf{r}_{O}^{n_{O}}\, \delta[z' - z(\mathbf{r}_{Si}^{n_{Si}})] \exp[-\beta U(\mathbf{r}_{Si}^{n_{Si}},\mathbf{r}_{O}^{n_{O}})]}{Z_{n_{Si},n_{O}}} \tag{5}$$

where Z_{n_{Si},n_O} is the configurational integral for the ring. The delta function restricts the integral to only those configurations with $z = z'$. Consequently, the right side of eq 5 is termed a restricted configurational integral where this integral is related to a free energy by

$$\beta F(z) = -\ln p(z) \tag{6}$$

The above free energy is a potential of mean force because the gradient of this potential with respect to z gives the force to flatten the ring, averaged over all configurations with z fixed.[24] The potential of mean force is also the reversible work to change z from a standard state to the fixed value.

3.4. Umbrella Sampling. In this work we compare the flatness parameter distributions in the crystal with those determined from unconstrained rings. Crystalline rings sample a different part of configuration space with respect to unconstrained rings because the configuration of crystalline rings is partially determined by the constraints imposed by bonds formed with neighboring atoms. Thus, sampling of the corresponding orientations by the unconstrained rings will have poor statistics. To overcome this problem we use umbrella sampling,[25] where a biasing function is included in the Hamiltonian. We are concerned with flat rings because it is these rings that circumscribe pores with large apertures. Consequently, the following parabolic biasing function is chosen

$$U_{bias}(z) = A(z - z_o)^2 \tag{7}$$

where A is a constant and z_o is the minimum in the biasing function. The full Hamiltonian is given by the sum of the biasing potential and the potential energy of the ring. With this Hamiltonian, rings will sample configurations with flatness parameter distributions close to $z = z_0$. The flatness parameter distributions determined with two different biasing Hamiltonians, H_1 and H_2, are related by

$$\ln p_2(z) = \ln p_1(z) + \beta[\Delta F - \Delta U_{bias}(z)] \tag{8}$$

where ΔF is the free energy of a ring with Hamiltonian H_2 minus that with Hamiltonian H_1 and $\Delta U_{bias}(z)$ is only a function of the flatness parameter. Using this formula and biasing potentials with different values of z_o, the flatness parameter distribution corresponding to the original potential can be patched together by fitting ΔF for pairs of systems corresponding to adjacent Hamiltonians.[26] For optimal results, there should be significant overlap in the corresponding flatness parameter distributions for the adjacent systems. For HBMC, we need to determine the force on each atom due to the biasing potential. The determination of this force is outlined in Appendix A.

4. Results and Discussion

4.1. Ring Size Distributions. The ring-size distributions for known zeolite structures and for the ensemble of 1800 hypothetical structures are shown in Figure 1. Of the known zeolite structures we use, only AET, CFI, DON, STF, SFF, and VFI contain channels circumscribed by rings containing more than 12 silica atoms. We have found that 14- and 18-membered fundamental rings occur in approximately 10% of the structures. However, these rings do not necessarily surround pores, and consequently many of these rings are not listed in zeolite databases. For instance, we find that sodalite contains fundamental 12-membered rings although the apertures in this material are formed by 6-membered rings only.

It is interesting to note from Figure 1 that there are very few odd-membered rings, even among hypothetical structures. This fact has long been appreciated for the known zeolites. The

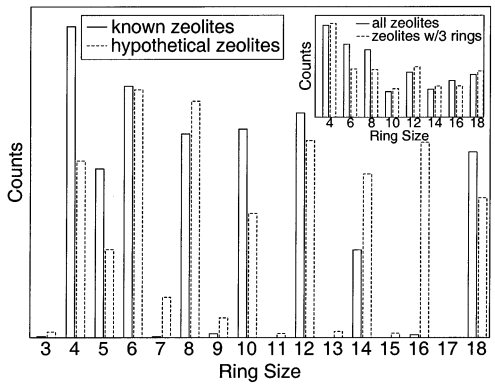

Figure 1. Ring-size distribution for known zeolite structures and for hypothetical structures generated using ZEFSAII with geometric terms only. The inset shows the ring-size distributions of hypothetical structures, comparing all hypothetical structures to hypothetical structures that contain at least one three-membered ring.

reason for the suppression of the odd-membered rings has been somewhat unclear. Energetically, there is no particular reason for even-membered rings to be favored over odd-membered rings.[9] What the histogram of hypothetical structures in Figure 1 shows is that it is the constraint of making a crystal from four-coordinated species that suppresses the odd-membered rings.

It has been shown that most zeolites have enthalpies of formation that fall within a narrow range of 6−14 kJ/mol Si greater than that of quartz. As pointed out by Helmkamp and Davis,[7] this is not surprising because all Si and O atoms are in similar environments; i.e., T-atoms are four-coordinated and O atoms are two-coordinated. In addition, all bond angles and bond lengths fall in a range over which there is only a small change in energy according to ab initio calculations on small model clusters. We expect that the zeolites generated using ZEFSAII have similar stabilities to known zeolites because crystal structures are weighted using potentials of mean force developed from known zeolite structures. Consequently, these structures should have typical bond lengths and angles and should fall in the same range of stabilities as given above. Furthermore, in general, correct zeolite structures are obtained by ZEFSAII in most cases without weighting according to diffraction data. Because all zeolites have similar stabilities, it is believed that controlling the kinetics is the main stumbling block to synthesizing zeolites with larger pores, and formation of many zeolites requires the use of structure-directing agents which are generally organocations. Here, we find that the ring-size distribution of the known zeolites is similar to that of the hypothetical structures except that a larger fraction of the rings in the hypothetical structures contain 14 and 16 members. This is in agreement with experimental observations that larger pores cannot be formed because the larger organocations that are required in the synthesis are not so easy to identify. Large organocations lead to either one or no structures, whereas smaller organocations can lead to multiple structures depending on the framework composition, countercations, and pH of the synthesis mixture.[3] On the basis of our results, it should be possible to choose synthesis conditions that favor the formation of 16-membered rings. A key recent insight along these lines is that not only does the organocation need to be energetically favorable for the desired product, but also it must be energetically unfavorable for competing zeolite species.[27]

Piccione et al.[8] and Henson et al.[28] have shown that a decrease in framework density is correlated with an increase in the enthalpy of formation for high-silica zeolites. Consequently, it might be expected that large rings are not thermodynamically stable because they are associated with large pores and a low framework density. While large, flat rings are less likely, this decreased likelihood turns out not to be primarily as a result of such a correlation. Only VFI has large rings and a significantly lower than average framework density. The known zeolites containing pores circumscribed by 14-membered rings (AET, CFI, and DON) have moderate framework densities with respect to other known zeolites. On the other hand, the zeolites containing 12-membered rings have the lowest densities. Indeed, when maximum ring size is plotted versus framework density for all the known zeolites, there is only a modest negative correlation.

Ring size distributions have been previously correlated with the densities of various silica polymorphs.[12,29] For instance, the most stable silicate is quartz, which contains only six- and eight-membered rings, and cristobalite has only six-membered rings. These silica polymorphs are twice as dense as typical zeolites. Because zeolites have a greater variety of ring sizes than does quartz or cristobalite, it might be expected that there is a correlation between framework density and the variance of the ring size distribution. From examining all known aluminosilicate zeolites, we find that the variance in the ring size distribution increases linearly with the average ring size of zeolites. On the other hand, surprisingly, there is only a modest negative correlation between framework density and the average ring size or the maximum ring size of a zeolite. Consequently, the variance of the ring size distribution is only modestly negatively correlated with the framework density. Similarly, while there is a strong negative correlation between the percentage of five-rings and the average ring size of a zeolite, there is only a modest positive correlation between the percentage of five-rings and the framework density of a zeolite.

In the inset of Figure 1, we show the histograms generated exclusively from hypothetical zeolites that contain three-membered rings. Brunner and Meier[30] have shown that there is a correlation between the minimum framework density and the smallest ring size in the framework. Thus, it has been proposed that zeolites containing three-membered rings may contain larger pores—i.e. three-membered rings may somehow help fill the gaps and holes created by large-membered rings. From Figure 1, we find that hypothetical zeolites containing three-membered rings do not have a larger number of 12, 14, or 18-membered rings. As mentioned above, zeolites containing 14-membered rings do not necessarily have a low framework density. On the other hand, the only zeolite with three-membered rings is MEI (ZSM-18), which has a relatively low density, and the largest ring contains only 12 members. All other molecular sieves with three-membered rings contain non-aluminosilicate framework T-atoms, such as Zn or Be.[31,32] The larger rings in these zeolites may be due to the potential energy curve for the T−O−Si bond angle, which has a minimum at a smaller angle than that of the Si−O−Si bond angle. Thus, it is not clear if three-membered rings in aluminosilicates will be associated with larger pores.

4.2. The Flatness of Rings. It is clear from Figure 1 that large rings occur in known zeolites. However, most of the large rings do not necessarily circumscribe pores with large openings. We use the flatness order parameter to assess the planarity of the rings. As mentioned earlier, the flatness parameter is unity for a planar ring and approaches zero for a spherical distribution of atoms in the ring. Flatness distribution histograms are given in Figure 2 for rings ranging in size from 4 to 18. The bars represent the flatness distributions of rings found in known zeolites. Rings that circumscribe pores are classified as tabulated

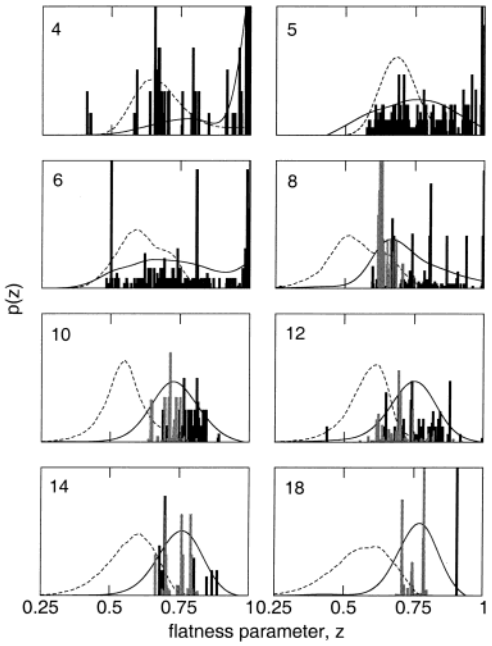

Figure 2. The flatness distributions for rings, where ring size is given in the corner of each figure. Solid lines refer to rings in hypothetical zeolite structures. Dark bars and light bars refer to tabulated and nontabulated rings, respectively, in known zeolites. Dashed lines refer to unconstrained rings. All curves are normalized to one, whereas the histograms are scaled for visual clarity.

and denoted by dark bars, and all other rings are given by the light bars. In general, rings that circumscribe pores have a larger value of the flatness parameter indicating these rings are more planar, as expected. A distribution of flatness parameters occurs because rings that circumscribe pores can be staggered. For instance, the 14-membered ring in CFI has a flatness parameter of about 0.7, whereas the 14-membered ring in DON has a flatness parameter of about 0.87. Consequently, the channel in CFI has dimensions of 7.2 × 7.5 Å and is smaller than that in DON, where the channel dimensions are 8.2 × 8.1 Å. Another example of the correlation between flatness and pore size is given by BEA, which contains a two-dimensional system of pores at right angles to each other. Both pores are circumscribed by 12-membered rings, although the apertures are different. The smaller opening of 5.5 × 5.5 Å is circumscribed by a ring with $z = 0.67$, whereas the larger opening of 7.6 × 6.4 Å is circumscribed by a ring with $z = 0.83$.

The solid lines in Figure 2 correspond to the distribution of the flatness parameter for rings in the hypothetical zeolites. The curves were fit using a cubic smoothing spline.[33] The flatness distributions of rings in known zeolites are similar to those in the hypothetical structures, indicating that the hypothetical structures provide a representative sample of zeolite structures. Because a large ensemble of rings is sampled in the hypothetical structures, we expect that the curves provide a measure of the free energy of a crystalline ring as a function of the flatness parameter. The 18-membered ring in VFI (VPI-5)[34] has a flatness parameter of about 0.9, which corresponds to a relatively unlikely ring according to the hypothetical distribution in Figure 2. Note that the ring histograms from Figure 2 shift to the left as a function of increasing ring size—i.e. the tail of the ring size distributions becomes smaller and $P(z = 1)$ becomes smaller with increasing ring size. Rings with a given, high value of the flatness parameter, therefore, become increasingly unlikely for larger ring sizes. VFI is an aluminophosphate, while parameters representative of aluminosilicates were used to generate the hypothetical distributions. It is possible that the flatness distributions of rings in aluminophosphates are different due to the differences in the force fields of aluminophosphates and aluminosilicates. For instance, VFI has a novel structure composed of "pinwheel" units, where the structure is stabilized by the octahedral coordination of Al.[35] The pinwheel structure is not observed in aluminosilicates, where the necessary Al chemistry is not possible. Most likely, it is this unusual coordination that allows VFI to attain an 18-ring with a flatness of $z = 0.9$. The only other tabulated 18-membered rings occur in STF (SSZ-35) and SFF (SSZ-44). However, these rings are not fundamental because they can be divided into sets of smaller rings. For this reason, the flatness of these rings is not shown in Figure 2. For reference, $z = 0.80$ and 0.79 for these rings in STF and SFF, respectively. According to Figure 2, these 18-membered rings are more likely than is the one in VFI. The 18-membered rings in SFF and STF circumscribe a pore opening with approximate dimensions of 12.5 × 9 Å,[6] which is considerably larger than the pore sizes in the zeolites containing pores circumscribed by 14-membered rings (DON, CFI, and AET).

The results of the HBMC simulations of unconstrained rings are given by the dashed lines in Figure 2. For all cases studied here, crystalline rings are flatter than unconstrained rings, although the flatness distributions of crystalline rings have some similarities to those of the unconstrained rings. For instance, the shapes of the flatness distributions for crystalline rings with 10−18 members are similar to those of the unconstrained rings, but shifted to larger z values. For unconstrained rings with six or eight members, it appears that the zeolite rings possess a flatter state. This state corresponds to the right shoulder of the flatness distributions of the unconstrained rings with six or eight members. For unconstrained rings with four or five members, the peak in the flatness distribution has completely shifted to the right indicating that most of these smaller rings occupy the flatter state. The crystalline rings, on the other hand, seem to be developing probability density near $z = 1$. The flatness distributions of both crystalline and unconstrained rings with six or eight members are skewed to the right. As ring size is decreased to four, a second peak corresponding to flat rings is observed. Because the flatness distributions of crystalline rings are similar to those of the unconstrained rings, we expect factors that determine the flatness of unconstrained rings are also significant for crystalline rings.

According to Figure 2, it appears that crystalline rings with five or more members have a finite probability of being planar, in contrast to the calculation on unconstrained rings. This is an artifact of symmetry. The positions of the atoms in the unit cell are determined by the unique atom positions and the symmetry operations. It is possible that the positions of the atoms on symmetry-related "special positions" are in the same plane as those of the unique atoms. However, in a crystal at finite temperature, the positions of the atoms are not fixed by symmetry. The atoms oscillate about the equilibrium positions according to the Debye−Waller factor, B

$$B = 8\pi^2\bar{u}^2 \tag{9}$$

where $\bar{u}^2$ is the mean square displacements of the atom. A typical value of B for zeolitic Si is 1 Å^2.[13] We have determined the flatness for different sized rings when the atoms oscillate about planar equilibrium positions. The results are given in Figure 3. The flatness distribution of the four-membered ring approaches a constant as $z \rightarrow 1$. As expected from the results of Appendix B, all other distributions vanish as $z \rightarrow 1$. As ring size increases, the corresponding flatness distributions shift to the right and

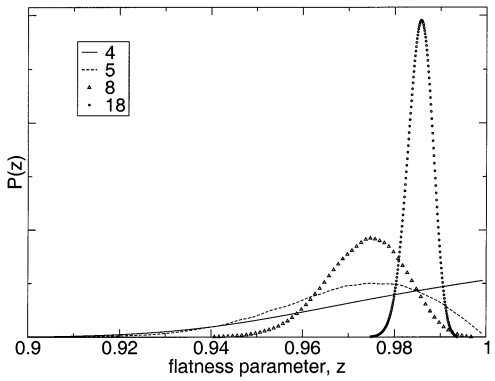

Figure 3. The flatness distributions for crystalline rings with thermal fluctuations given by a Debye−Waller factor of $B = 1$ Å^2. Ring size is given in the legend.

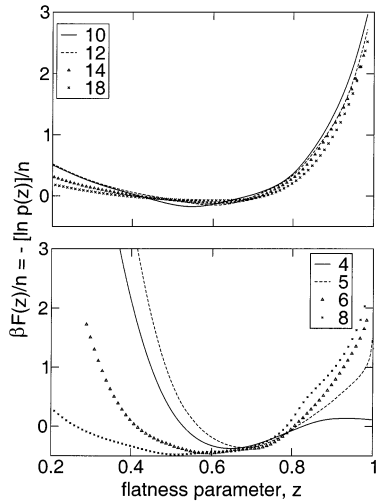

Figure 4. Free energy of an isolated ring as a function of the flatness of the ring, where the numbers in the legend denote ring size.

become narrower because the flatness parameter is measuring the size of thermal fluctuations relative to the ring size. Note again that Figure 3 is showing the Debye−Waller fluctuations about an otherwise "flat" ring.

4.3. Free Energies of Rings with Defined Flatness. Figure 4 gives the natural logarithm of the flatness distributions as determined with umbrella sampling for all possible values of *z*. These curves are reduced by the ring size, where the ring size corresponds to the number of SiO_4 units contained in the ring. In general, these units behave as rigid tetrahedra: the O−T−O angle is much less flexible than the T−O−T angle, which can accommodate angles in the range of 130° and 180°. According to the reversible work theorem, the slope of the curves in Figure 4 gives the average force per tetrahedra to flatten the rings. For ring sizes of 10 and above, the free energy curves are very similar, indicating that the SiO_4 tetrahedra are in similar environments irrespective of the size of the ring. For rings of eight-members and below, the average force to flatten the ring per tetrahedra decreases with decreasing ring size.

Note from Figure 4 that the probability to observe rings with higher values of the flatness parameter is lower, since this probability is proportional to the negative exponential of the free energy. As rings that span channels or windows become larger, the flatness parameter typically increases, because *z* is one minus the ratio of the shortest length to the longest length of the ring, and the longest length increases as the diameter of the ring increases. Hence, one reason that larger, pore- or window-spanning rings are less likely is that they are typically

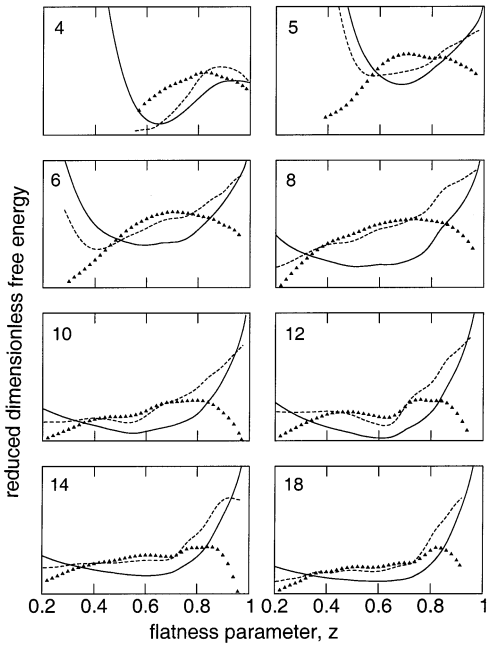

Figure 5. The thermodynamic properties of unconstrained rings as a function of flatness where the solid lines give the free energy, dashed lines gives the internal energy, and triangles give the entropy. Ring size is given in the corner of each figure.

flatter, and flatter rings are less likely. Moreover, larger rings are exponentially less likely than smaller rings of the same flatness, since the free energy per ring in Figure 4 is proportional to ring size for large rings. In Figure 4, the *y*-axis is free energy divided by ring size, and the curves for large ring size are all roughly the same; hence free energy per ring is proportional to ring size for large rings.

More insight can be gained by decomposing the free energy of the unconstrained rings into the sum of an entropic and an energetic contribution using the thermodynamic relation

$$\beta F(z) = \beta E(z) - \frac{S(z)}{k_B} \tag{10}$$

The thermodynamic quantities of eq 10 are related to restricted configurational integrals and consequently are a function of the flatness parameter, *z*. The potential of mean force $F(z)$ is plotted in Figure 4. We determine $E(z)$ from the simulations using histogram methods. The entropy term, $S(z)$, is then determined by subtracting the $F(z)$ curve from the $E(z)$ curve. The results are given in Figure 5.

The internal energy of a free ring is primarily determined by the short-range two-body and three-body forces, i.e. the distribution of bond angles and bond lengths. For unconstrained rings of five members and higher, we find $\theta_{Si-O-Si} = 144.1° \pm 8.3°$, $\theta_{O-Si-O} = 110.0° \pm 4.3°$, and $r_{Si-O} = 1.674 \pm 0.044$. These results are similar to bond angles and bond lengths obtained from ab initio calculations on clusters,[14] distributions in amorphous silica,[29] and in various zeolites.[36] The four-membered rings have slightly different values, given by $\theta_{Si-O-Si} = 139.3° \pm 7.5°$, $\theta_{O-Si-O} = 108.7° \pm 4.1°$, and $r_{Si-O} = 1.684 \pm 0.045$. The slightly lower values of the bond angles indicate ring cyclization introduces strain in four-membered rings. This is consistent with the finding that four-membered rings are less likely to be observed in amorphous silica,[29] although we find that there is an abundance of four-membered rings in known zeolite structures. Favorable interactions are maximized in the compact spherical state as opposed to the planar extended states,

where distance to neighbors is at a maximum. These favorable interactions most likely originate from the long-ranged dipolar and dispersion forces because bond angles and bond lengths are relatively independent of z. Thus, $U(z)$ generally increases as the ring is flattened. Exceptions to this behavior occur for small rings, where steric overlap prevents the rings from folding to spherical states.

The entropic contribution to the free energy of the ring is as significant as the energetic contribution. Because we do not use an explicit model for water, this entropy is only configurational. As shown in Figure 5, the entropy of the ring has a maximum at an intermediate value of z for all ring sizes. As $z \rightarrow 0$, entropy decreases because the volume available to compact ring configurations is small. In the other limit of $z \rightarrow 1$, the restricted entropy diverges to $-\infty$ in all cases other than four-membered rings. The divergence of the ring entropy as $z \rightarrow 1$ is a result of reducing the available T-atom phase space from a volume to a surface. The ring entropy in the limit of $z \rightarrow 1$ depends on the ring size. For rings with 3 T-atoms, $z = 1$ for all configurations because three points define a plane. As shown in Appendix B, as $z \rightarrow 1$, rings with 4 T-atoms have a finite entropy, whereas the entropy diverges for all rings with greater than four-members. Thus, we expect that the entropy is a function of ring size for relatively small rings.

On the other hand, for infinitely large rings, the reduced thermodynamic properties should be independent of ring size, where the reduced properties are equal to those of the chemically equivalent linear form. This behavior is observed for rings with 10−18 members, as shown in Figure 4, where the corresponding reduced free energy curves are similar. These curves have a steep increase for $z > 0.9$ due to the entropic contribution of the backbone atoms. This behavior is also observed for crystalline rings; the flatness distributions of rings with 10−18 members are similar. Furthermore, very few of these rings have $z > 0.9$. The transition from infinitely large rings to planar three-membered rings occurs for rings with between four and eight members. For these rings, the cyclic constraint favors planar structures, and planar rings of this size occur in zeolites.

4.4. The Free Energy Associated with Crystallization of Rings. We have found that flatness distributions of unconstrained rings are correlated with those of crystalline rings, indicating that similar forces occur in unconstrained rings and in crystalline rings. However, in all cases, crystalline rings are flatter than unconstrained rings due to the constraints imposed by the surrounding crystal. These constraints can be quantified in terms of an averaged crystalline potential if we assume that the set of all rings contained in the hypothetical zeolites provides a representative sample of all zeolite structures. With this assumption, the flatness distribution of crystalline rings is related to a potential of mean force in a manner analogous to eq 6. For the present case, the definition of the corresponding probability distribution involves averaging over the positions of atoms in the ring as well as in the surroundings, consistent with a given z. The average behavior of the surrounding atoms flattens the ring, as observed in Figure 2. This behavior can be related to an averaged crystalline potential using a reverse umbrella sampling technique. Rearranging eq 8 gives

$$\beta U_{\text{cryst}}(z) = \ln \frac{p(z)}{p_{\text{cryst}}(z)} + \beta \Delta F \qquad (11)$$

where $p_{\text{cryst}(z)}$ refers to the flatness distribution in the crystal, $p(z)$ refers to the flatness distribution of the unconstrained ring, and $U_{\text{cryst}}(z)$ is the averaged crystalline potential. The crystalline potential is the average change in energy of the surroundings as a function of the flatness of the ring. This energy includes the two-body and three-body forces between the terminal oxygen groups of the ring and the surroundings as well as all other interactions involving atoms in the surroundings. The quantity $\beta \Delta F$ is the free energy of an unconstrained ring minus that of a ring immersed in the crystalline potential field, $U_{\text{cryst}}(z)$. This free energy term is independent of the flatness parameter because the free energy is determined from integrating over all flatness configurations. The function $U_{\text{cryst}}(z)$ is given in Figure 6.

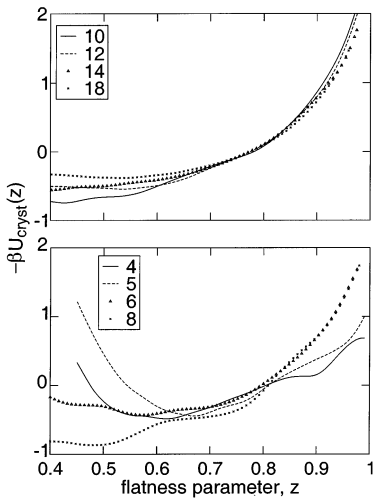

Figure 6. The crystal energy function plotted versus the flatness parameter. Ring size is given in the legend.

For ring sizes of 10−18, the flatness of the ring typically varies from 0.6 to 0.9 in the hypothetical crystal structures. Rings of low flatness are similar to unconstrained rings, where a more compact state maximizing nonbonded interactions between the atoms on the ring is favored. On the other hand, the effect of the crystal is to stretch the ring by favorable interactions between the ring and the surroundings. A change in z from 0.6 to 0.9 corresponds to $\Delta U_{\text{cryst}}(z) = 5$ kJ/mol Si, which is similar to the range of stabilities observed for all-silica zeolites. According to Petrovic et al.,[36] less stable all-silica zeolites contain bond angles where $\theta_{\text{Si-O-Si}} < 135°$, and for Si−O−Si bond angles below 135°, there is a steep increase in the three-body potential as calculated from ab initio calculations.[17] This result seems to indicate that intramolecular interactions between atoms on the ring favor a nonflat ring that allows less strained bond angles. As examples, the zeolites MTW (ZSM-12), EMT, and FAU have populations of Si−O−Si bond angles where $\theta_{\text{Si-O-Si}} < 140°$. All of these zeolites contain nonplanar 12-membered rings with flatness parameters less than 0.65. However, nonflat rings are more likely to have strained bond angles with the surroundings due to the proximity of the terminal groups. This strain can be minimized by stretching the ring. Another possible source for the energetic stabilization of flat rings is interaction with structure directing agents. Piccione et al.[37] have shown that the interaction between the zeolite frameworks and organocations is on the order of 3−9 kJ/mol Si in most cases. It is possible that the interaction between flat rings and the "templating" molecule are significant and that it is these interactions which stabilize the formation of large pores. Conversely, nonflat rings usually do not necessarily interact with the structure directing agents because these rings do not usually circumscribe pores.

5. Conclusions

In this work, we have surveyed the size and flatness of rings that occur in known zeolites and also in a set of hypothetical

structures. We have found that many large rings exist in known zeolites, although these rings do not necessarily circumscribe pores. We have defined a flatness parameter to distinguish between rings that circumscribe pores and rings that do not surround pores. Comparison of the flatness distributions of known zeolites to those of the hypothetical zeolites shows that it should be possible to synthesize zeolites containing at least somewhat flat rings with greater than 12 members. Our results suggest that the main stumbling block in the formation of large pores is not thermodynamics but rather identification of suitable organocations as templating agents.

We have also investigated the thermodynamic factors that influence the flatness of crystalline rings. The thermodynamic properties of a crystalline ring can be decomposed into a contribution from the unconstrained ring and a contribution from the interaction between the unconstrained ring and the surroundings. There is an entropic barrier to forming planar rings, which increases with increasing ring size and becomes significant for rings with 10 or more members. This entropic effect is balanced by an averaged crystalline field that stretches the ring, most likely by relieving strained bond angles or possibly by forming interactions between a structure directing agent and the ring. The energy required to form roughly planar crystalline rings from the unconstrained state is 5 kJ/mol Si, roughly the interaction energy between zeolites and structure directing agents and also roughly the range of stabilities of zeolites. In support of this hypothesis, it may be interesting to correlate the degree of energetic interaction between structure directing agent and zeolite with the degree of structural relaxation of the zeolite framework after calcination.

Acknowledgment. This work was supported by the Chevron Research and Technology Company, the donors of the Petroleum Research Fund, the Department of Energy, and the National Science Foundation. We are pleased to acknowledge helpful discussions with Mark E. Davis and Stacey I. Zones.

Appendix A: Calculation of the Force Due to the Biasing Potential

In this Appendix, we derive an analytical expression for the force on particle k due to the biasing potential. The γ-component of this force is given by

$$F_k^\gamma = -2A(z - z_o)\frac{dz}{dr_k^\gamma} \tag{A-1}$$

The derivative on the right side of eq 1 can be evaluated from the definition of the flatness parameter, $z = 1 - (\lambda_3/\lambda_1)^{1/2}$

$$\frac{dz}{dr_k^\gamma} = -\frac{1}{2(\lambda_1\lambda_3)^{1/2}}\frac{d\lambda_3}{dr_k^\gamma} + \frac{\lambda_3^{1/2}}{2\lambda_1^{3/2}}\frac{d\lambda_1}{dr_k^\gamma} \tag{A-2}$$

where

$$\frac{d\lambda_i}{dr_k^\gamma} = \sum_{\alpha,\beta}\frac{\partial\lambda_i}{\partial M^{\alpha\beta}}\frac{\partial M^{\alpha\beta}}{\partial r_k^\gamma} \tag{A-3}$$

The sum in eq A-3 is over all elements of the T-atom distribution matrix, $M^{\alpha\beta}$. Note that Roman subscripts are used to label eigenvalues, eigenvectors, and atom identity. Greek superscripts refer to Cartesian coordinate index. The derivative $\partial\lambda_i/\partial M^{\alpha\beta}$ can be evaluated by considering a small perturbation to M:

$$(M + \epsilon)(\mathbf{x} + \delta\mathbf{x}) = (\lambda + \delta\lambda)(\mathbf{x} + \delta\mathbf{x}) \tag{A-4}$$

where ϵ is a null matrix except for element, $\epsilon^{\alpha\beta} = \delta M^{\alpha\beta}$. The quantities $\mathbf{x} + \delta\mathbf{x}$ and $\lambda + \delta\lambda$ are the sets of eigenvectors and eigenvalues corresponding to the matrix $M + \epsilon$. Associativity of eq A-4 gives

$$M\delta\mathbf{x}_i + \epsilon\mathbf{x}_i = \lambda_i\delta\mathbf{x}_i + \delta\lambda_i\mathbf{x}_i \tag{A-5}$$

where we have neglected second-order perturbation terms and used the matrix relation $M\mathbf{x}_i = \lambda_i\mathbf{x}_i$. Equation A-5 can be multiplied by $\mathbf{x}_i^T$ to give

$$\mathbf{x}_i^T M\delta\mathbf{x}_i + \mathbf{x}_i^T\epsilon\mathbf{x}_i = \mathbf{x}_i^T\lambda_i\delta\mathbf{x}_i + \delta\lambda_i \tag{A-6}$$

using the orthonormality property of the eigenvectors. Further simplification follows from substitution of $\mathbf{x}_i^T M = \lambda_i\mathbf{x}_i^T$ into eq A-6:

$$\delta M^{\alpha\beta}x_i^\alpha x_i^\beta = \delta\lambda_i \tag{A-7}$$

The desired result follows immediately

$$\frac{\partial\lambda_i}{\partial M^{\alpha\beta}} = x_i^\alpha x_i^\beta \tag{A-8}$$

where x_i^α is the α-component of eigenvector $\mathbf{x}_i$.

The definition of the matrix M gives for each element $M^{\alpha\beta}$

$$M^{\alpha\beta} = \sum_i r_i^\alpha r_i^\beta - \frac{1}{N}\sum_i r_i^\alpha\sum_j r_j^\beta \tag{A-9}$$

Straightforward calculus shows that

$$\frac{\partial M^{\alpha\beta}}{\partial r_k^\gamma} = \delta_{\gamma\alpha}\left(r_k^\beta - \frac{1}{N}\sum_i r_i^\beta\right) + \delta_{\gamma\beta}\left(r_k^\alpha - \frac{1}{N}\sum_i r_i^\alpha\right) \tag{A-10}$$

where $\delta_{\alpha\beta}$ is the Kronecker delta that is equal to 1 if $\alpha = \beta$ and is equal to 0 if $\alpha \neq \beta$. Substitution of eqs A-10, A-8, and A-3 into eq A-2 gives

$$\frac{dz}{dr_k^\gamma} = \sum_\alpha\left[-\frac{x_3^\alpha x_3^\gamma}{(\lambda_1\lambda_3)^{1/2}} + \frac{\lambda_3^{1/2}x_1^\alpha x_1^\gamma}{\lambda_1^{3/2}}\right]\left[r_k^\alpha - \frac{1}{N}\sum_i r_i^\alpha\right] \tag{A-11}$$

Equation A-11 is used to calculate the force on atom k according to eq A-1.

Appendix B: Demonstration that $P(z = 1)$ Vanishes for Ring Sizes Greater than Four

In this Appendix, we show that the probability distribution $P(z = 1)$ vanishes for ring sizes, N, greater than four. We first note that all atoms of the ring must lie in a plane when $z = 1$. Without loss of generality, we choose a rotated coordinate system in which the first three silicon atoms lie in the $x-y$ plane. We then consider the z-components of silicon atoms 4, ..., N to be small, so that the ring is nearly flat. The definition of the flatness parameter distribution from eq 5 then becomes

$$p(z') = Z_{n_{Si},n_O}^{-1}\int d\mathbf{r}'\, dz_4 \ldots dz_N\,\delta\,[z' - z(\mathbf{r}_{Si}^N)]\,\exp[-\beta U] \tag{B-1}$$

where $\mathbf{r}'$ includes the x, y components of silicon atoms 4, ..., N in the ring and the positions of all of the oxygen atoms and of

all of the other silicon atoms not in the ring. We first evaluate the part of the integral that involves z_4, ..., z_N. We note from eqs 2 and 3 that the flatness parameter is given by

$$z = 1 - \frac{(z_4^2 + ... + z_N^2)^{1/2}}{\lambda_1(x_1, y_1, ..., x_N, y_N)^{1/2}} \quad \text{(B-2)}$$

to first order in the z-components. Using eq B-2 in eq B-1, we find

$$p(1) = Z_{n_{Si},n_O}^{-1} \int d\mathbf{r}' \exp[-\beta U]\, dz_4 ... dz_N\, \delta [(z_4^2 + ... + z_N^2)^{1/2}/\lambda_1^{1/2}] \quad \text{(B-3)}$$

Performing the integration in $dz_4 ... dz_N$ via spherical coordinates in $N - 3$ dimensions, we find

$$p(1) = Z_{n_{Si},n_O}^{-1} \int d\mathbf{r}' \exp[-\beta U]\lambda_1^{1/2} S_{N-3} \int_0^\infty r^{N-4}\, dr\, \delta(r) \quad \text{(B-4)}$$

where $S_d = 2\pi^{d/2}/\Gamma(d/2)$ is the surface area in d dimensions and $\Gamma(x) = (x - 1)!$ is the Gamma function. Using the identity $\delta(x) = \lim_{a\to\infty} (1/2)a \exp(-a|x|)$, we find

$$p(1) = Z_{n_{Si},n_O}^{-1} \int d\mathbf{r}' \exp[-\beta U]\, \lambda_1^{1/2} \frac{S_{N-3}}{2} \lim_{a\to\infty} \int_0^\infty r^{N-4}\, dr\, ae^{-ar}$$

$$= Z_{n_{Si},n_O}^{-1} \int d\mathbf{r}' \exp[-\beta U]\, \lambda_1^{1/2} \frac{S_{N-3}}{2} \lim_{a\to\infty} \frac{a\Gamma(N-3)}{a^{N-3}} \quad \text{(B-5)}$$

This expression vanishes when $N \geq 5$. When $N = 4$, this expression reduces to a finite value. Summarizing these results, we find

$$P(z = 1) = \begin{cases} \delta(z - 1), N = 3 \\ \text{const}, N = 4 \\ 0, N \geq 5 \end{cases} \quad \text{(B-6)}$$

This result is evident in the probability distributions of Figure 3 and in the free energy curves of Figure 4.

References and Notes

(1) Davis, M. E. *Chem. Eur. J.* **1997**, *3*, 1745.
(2) Davis, M. E. *Nature* **2002**, *417*, 813.
(3) Zones, S. I.; Nakagawa, Y.; Lee, G. S.; Chen, C. Y.; Yuen, L. T. *Microporous Mesoporous Mater.* **1998**, *21*, 199.
(4) Wessels, T.; Baerlocher, C.; McCusker, L. B.; Creyghton, E. J. *J. Am. Chem. Soc.* **1999**, *121*, 6242.
(5) Yoshikawa, M.; Wagner, P.; Lovallo, M.; Tsuji, K.; Takewaki, T.; Chen, C.-Y.; Beck, L. W.; Jones, C.; Tsapatsis, M.; Zones, S. I.; Davis, M. E. *J. Phys. Chem. B* **1998**, *102*, 7139.
(6) Wagner, P.; Zones, S. I.; Davis, M. E.; Medrud, R. C. *Angew. Chem., Int. Ed.* **1999**, *38*, 1269.
(7) Helmkamp, M. M.; Davis, M. E. *Annu. Rev. Mater. Sci.* **1995**, *25*, 161.
(8) Piccione, P. M.; Laberty, C.; Yang, S.; Camblor, M. A.; Navrotsky, A.; Davis, M. E. *J. Phys. Chem. B* **2000**, *104*, 10001.
(9) Wu, G.; Deem, M. W. *J. Chem. Phys.* **2002**, *116*, 2125.
(10) Falcioni, M.; Deem, M. W. *J. Chem. Phys.* **1999**, *110*, 1754 (http://www.mwdeem.rice.edu/zefsaII).
(11) Deem, M. W.; Newsam, J. M. *J. Am. Chem. Soc.* **1992**, *114*, 7189.
(12) Stixrude, L.; Bukowinski, M. S. T. *Am. Mineral.* **90**, *75*, 1159.
(13) Baerlocher, C. H.; Meier, W. M.; Olson, D. H. *Atlas of Zeolite Framework Types*; Elsevier: Amsterdam, 2001 (http://www.iza-structure-.org/).
(14) Nedelec, J. M.; Hench, L. L. *J. Non-Cryst. Solids* **1999**, *255*, 163.
(15) Pereira, J. C. G.; Catlow, C. R. A.; Price, G. D. *J. Phys. Chem. A* **1999**, *103*, 3252.
(16) Moravetski, V.; Hill, J.-R.; Eichler, U.; Cheetham, A. K.; Sauer, J. *J. Am. Chem. Soc.* **1996**, *118*, 13015.
(17) Gibbs, G. V. *Am. Mineral.* **1982**, *67*, 421.
(18) Blake, N. P.; Weakliem, P. C.; Metiu, H. *J. Phys. Chem. B* **1998**, *102*, 67.
(19) Hill, J.-R.; Sauer, J. *J. Phys. Chem.* **1994**, *98*, 1238.
(20) Tsuneyuki, S.; Tsukada, M.; Aoki, H.; Matsui, Y. *Phys. Rev. Lett.* **1988**, *61*, 869.
(21) Vashishta, P.; Kalia, R. K.; Rino, J. P.; Ebbsjö, I. *Phys. Rev. B* **1990**, *41*, 12197.
(22) Koudriachova, M. V.; Beckers, J. V. L.; de Leeuw, S. W. *Comput. Mater. Sci.* **2001**, *20*, 381.
(23) Brotz, F. A.; de Pablo, J. *Chem. Eng. Sci* **1994**, *49*, 3015.
(24) Chandler, D. *Introduction to Modern Statistical Mechanics*; Oxford University Press: New York, 1987.
(25) Torrie, G. M.; Valleau, J. P. *J. Comput. Phys.* **1977**, *23*, 187.
(26) Bader, J. S.; Chander, D. *J. Phys. Chem.* **1992**, *96*, 6423.
(27) Wagner, P.; Nakagawa, Y.; Lee, G. S.; Davis, M. E.; Elomari, S.; Medrud, R. C.; Zones, S. I. *J. Am. Chem. Soc.* **2000**, *122*, 263.
(28) Henson, N. J.; Cheetham, A. K.; Gale, J. D. *Chem. Mater.* **1994**, *6*, 1647.
(29) Rino, J. P.; Ebbsjö, I.; Kalia, R. K.; Nakano, A.; Vashishta, P. *Phys. Rev. B* **1993**, *47*, 3053.
(30) Brunner, G. O.; Meier, W. M. *Nature* **1989**, *337*, 146.
(31) Annen, M. J.; Davis, M. E.; Higgins, J. M.; Schlenker, J. L. *J. Chem. Soc. Chem. Commun.* **1991**, 1175.
(32) Annen, M. J.; Davis, M. E. *Microporous Mater.* **1993**, *1*, 57.
(33) Lancaster, P.; Salkauskas, K. *Curve and Surface Fitting*; Acaemic Press: New York, 1986.
(34) Davis, M. E.; Saldarriaga, C.; Montes, C.; Garces, J.; Crowder, C. *Nature* **1988**, *331*, 698.
(35) Li, H.-X.; Davis, M. E. *Catalysis Today* **1994**, *19*, 61.
(36) Petrovic, I.; Navrotsky, A.; Davis, M. E.; Zones, S. I. *Chem. Mater.* **1993**, *5*, 1805.
(37) Piccione, P. M.; Yang, S.; Navrotsky, A.; Davis, M. E. *J. Phys. Chem. B* **2002**, *106*, 3629.